International Journal of Thermophysics, Vol. 23, No. 1, January 2002 (© 2002)

Gas "Wets" a Solid Wall in Orbit[1]

J. Hegseth,[2,3] Y. Garrabos,[4] V. S. Nikolayev,[4] C. Lecoutre-Chabot,[4] R. Wunenburger,[4] and D. Beysens[4]

When coexisting gas and liquid phases of a pure fluid are heated through their critical point, large-scale density fluctuations make the fluid extremely compressible and expandable and slow the diffusive transport. These properties lead to perfect wetting by the liquid phase (zero contact angle) near the critical temperature T_c. However, when the system's temperature T is increased to T_c, so that it is slightly out of equilibrium, the apparent contact angle is very *large* (up to 110°), and the *gas* appears to "wet" the solid surface. These experiments were performed and repeated on several missions on the Mir space station using the Alice-II instrument, to suppress buoyancy-driven flows and gravitational constraints on the liquid–gas interface. These unexpected results are robust, i.e., they are observed under either continuous heating (ramping) or stepping by positive temperature quenches, for various morphologies of the gas bubble and in different fluids (SF_6 and CO_2). Possible causes of this phenomenon include both a surface-tension gradient, due to a temperature gradient along the interface, and the vapor recoil force, due to evaporation. It appears that the vapor recoil force has a more dominant divergence and explains qualitatively the large apparent contact angle far below T_c.

KEY WORDS: contact angle; critical exponent; Marangoni flow; principal axis; surface tension; thermal-capillary flow; vapor recoil.

1. INTRODUCTION

When a coexisting liquid–gas mixture of a single species fluid is heated into the gas phase, a complex process of fluid dynamics, heat transfer, and

[1] Paper presented at the Fourteenth Symposium on Thermophysical Properties, June 25–30, 2000, Boulder, Colorado, U.S.A.

[2] Department of Physics, University of New Orleans, New Orleans, Louisiana 70148, U.S.A.

[3] To whom correspondence should be addressed. E-mail: jhegseth@uno.edu

[4] ESEME, Institut de Chimie de la Matière Condensée de Bordeaux, CNRS, Université de Bordeaux I, Avenue du Dr. Schweitzer, F-33608 Pessac Cedex, France.

0195-928X/02/0100-0089/0 © 2002 Plenum Publishing Corporation

interfacial phenomena usually occurs [1]. This process, often called boiling, is important in many applications because of the large heat transfer that it can facilitate, so many types of heat transfer technology use this process. Many of these complications are caused by the buoyancy from gravity, which lifts the gas bubbles that nucleate on a hot surface. Near the liquid–gas critical point, material and thermal properties that play an important roll in the boiling process such as the surface tension vary considerably with temperature [2]. These properties vary according to well-known universal power laws that either converge or diverge (e.g., the surface tension goes to zero) and lead to perfect wetting by the liquid phase (zero contact angle) near the critical temperature T_c [3]. In a boiling process, we can expect a perfectly wetted wall to dry from evaporation, resulting in liquid–gas–solid contact lines. The same physics that makes perfect wetting in equilibrium will result in a boundary condition of zero contact angle when heat is applied. Here we report on observations of a single bubble in a thin constant mass cell that is filled with fluid very close to its critical density. This thin cell produces a considerable constraint on the bubble and allows the entire bubble to be observed as the heat is applied. As the liquid–gas mixture is heated toward the critical point, the diverging and converging material properties produce a large effect on the bubble shape.

2. RESULTS

In these experiments, a thin layer of SF_6 or CO_2 was sandwiched between two sapphire windows and surrounded by a copper housing in the optical cell shown in Fig. 1. Figures 2 and 3 show the results from a typical run where the cell was heated linearly in time to a temperature higher than the critical temperature T_c while the liquid–gas interface was visualized through light transmission normal to the windows. Figure 3 shows several cell images obtained during the heating. Because the contact angle is zero near the critical point, the liquid–gas meniscus between the two parallel windows forms a semicircular interface in the plane perpendicular to the windows. The interface appears dark in the images because the liquid–gas meniscus refracts the normally incident light away from the cell axis. We have verified by a ray-tracing model that all of the normally incident light on the meniscus is refracted out of the field of view. This shows that in normally incident light, the dark region measures the radius of the semicircular meniscus.

These results were obtained and repeated using several samples of both SF_6 and CO_2 under different cell aspect ratios and heating protocols (ramping rates and quenches) on several French/Russian (Cassiopée and

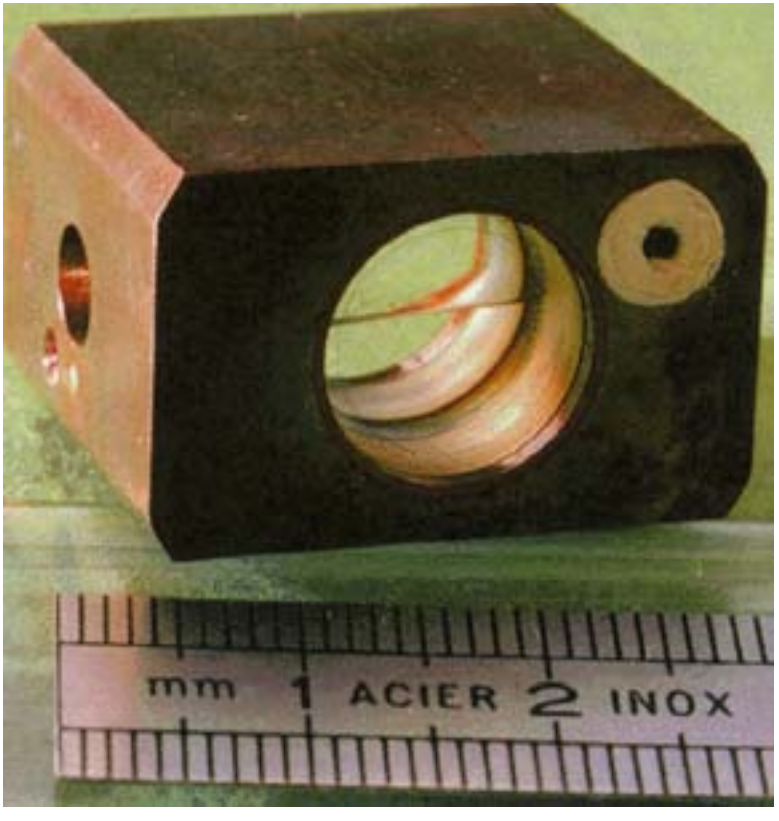

Fig. 1. Sample cell. Shown is the sample cell in terrestrial gravity filled with SF_6 fluid. The meniscus between the coexisting liquid and gas phases below the critical point can be seen. The average density exceeds the critical density by $0.3 \pm 0.01\%$. The fluid volume (12.000-mm diameter, 1.664-mm thickness) is contained between two sapphire windows and a CuBeCo alloy housing.

Pegase) and French/American (GMSF) missions on the Mir space station using the Alice-II instrument [4]. This instrument is specially designed to obtain high-precision temperature control (stability of ≈ 10 μK over 50 h, repeatability of ≈ 40 μK over 7 days). To place the samples near the critical point, constant-mass cells are prepared with a high-precision density, to 0.02%, by observing the volume fraction change of the cells as a function of the temperature on the ground [5]. Two cylindrical sapphire windows 12 mm in diameter and 90 mm long are pressed into a copper block with a corresponding cylindrical hole and glued to the copper at the sides of the sapphire. This method avoids the unknown volume associated with o-rings, etc., allowing the above-high-precision density measurements to be verified.

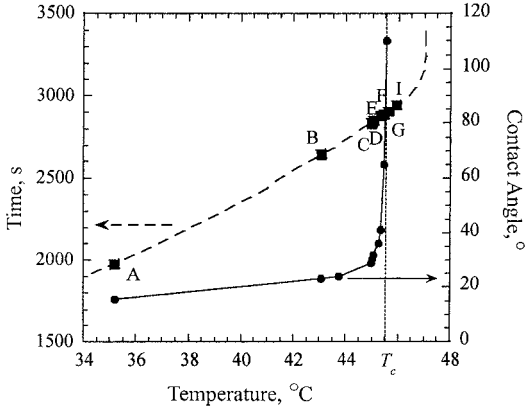

Fig. 2. Plots of the contact angles as a function of temperature and the temperature of the cell as a function of time. The critical temperature of SF_6 is $T_c = 45.54°C$ as shown. The mean value of dT/dt at T_c is about 8.4 $mK \cdot s^{-1}$. Also shown are points where the images in Fig. 3 were taken, with the corresponding letter labels.

We also note that some of the fluid volume near the cell edge is not visible in our images because it is blocked by glue. This radial edge distance is approximately 1 mm. Nevertheless, we can find the cell center and cell edge because there is a 10-mm-diameter reference etching on the sapphire windows that is concentric with the cell. Similar ground-based experiments were done before these experiments, yielding completely different results [5]. In this case the interface is horizontal except very near a wall.

In our system the liquid wets the solid, so that the initial state of our system before heating is a flat bubble constrained by the two windows and the cell edge. The initial off-center position of the bubble, with part of the bubble touching the copper ring, occurs because the cell windows are not exactly parallel and constrain the bubble to press against the ring. We can estimate the tilt angle, θ, between the windows from the mechanical precision of the cell manufacturing process, and it does not exceed 0.3°. In thicker cells when the bubbles are not pressed against the ring or when the bubble is constrained not to touch the side wall, no similar bubble deformation is observed.

Figures 2 and 3 show that as the critical point is approached, the gas region spreads along the copper side wall. Because the curvature on a large portion of the bubble is constant, we can extrapolate it to the wall to define an apparent contact angle (see Fig. 3A), and this apparent contact angle increases. The dark region that measures the meniscus radius does not

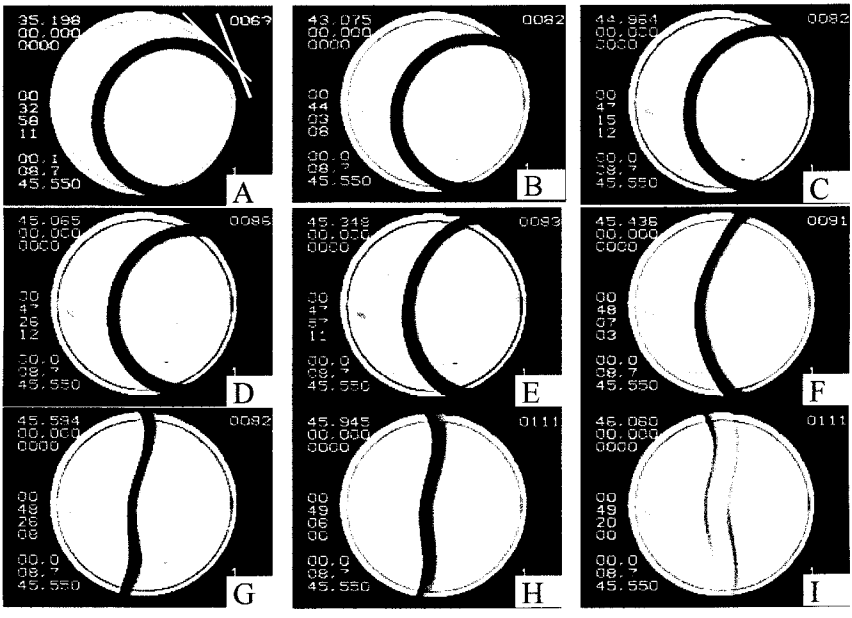

Fig. 3. Contact angle and bubble shape. Shown is a series of images of the bubble at various temperatures indicated in Fig. 2. (A) A thin line that estimates the tangent to the bubble at the cell edge. The apparent contact angle is the angle between this thin line and the thick line that indicates the tangent to the cell's edge (the cell's edge is out of the field of view). The change in the contact angle and bubble shape is clearly seen. The first row of images shows that the bubble distortion and contact angle changes occur even far below the critical point. The second row of images illustrates the rapid changes that occur close to the critical point. The last row of images shows a density gradient that replaces the interface above the critical temperature.

appear to be significantly affected except at the side wall, where it disappears. Figures 2 and 3 show that there is a significant bubble deformation quite far below the critical temperature T_c. Near the critical temperature the gas has spread over nearly half the copper side wall. The apparent contact angle becomes so large that the gas phase appears to "wet" a large portion of the cell surface. When crossing the critical point, as shown in Figs. 3D–H, the vapor bubble loses its convexity and rapidly evolves. At $T \approx T_c$, there is no latent heat and no surface tension so that the interface becomes a density gradient. This is shown in the last several images in Fig. 3.

3. DISCUSSION

Figures 2 and 3 show that there is significant bubble deformation below T_c where the surface tension is still relatively high and the shape may

be analyzed by quasi-static arguments. If a temperature change, δT, appears along the liquid–gas interface, it will create a surface-tension gradient $\delta\sigma = (\mathrm{d}\sigma/\mathrm{d}T)\,\delta T$ that will drive a thermal capillary or a Marangoni flow in the bulk of both fluids [6–8]. Such a flow could modify the shape of the bubble. We have previously seen Marangoni rolls in similar cells in the same apparatus in ground-based experiments using the shadowgraph effect. These rolls have a horizontal width of the order of the cell thickness and are transient. They form near the gas–liquid interface after a large temperature quench and travel along the horizontal interface for several seconds before disappearing.

One of us (J.H.) has also seen similar shadowgraph images of sustained Maranogoni convection in evaporating methanol along a thin horizontal interface in similar geometry verifying that the transient rolls are Marangoni rolls, probably also driven by evaporation. We have not seen any evidence of the steady convection that is required to create and maintain the observed bubble shape in our experiments. We have, however, on occasion seen transient plumbs in some experimental runs from bubble coalescence, but these events had only a small transient influence on the bubble shape. The fact that there is no convection farther away from the critical point shows that the interface is isothermal. This may not necessarily be true closer to the critical point.

The dimensionless parameter that governs the stability of an isothermal interface, in the presence of an externally imposed temperature gradient normal to the interface, is the Marangoni number, given by $\mathrm{Ma} = \delta\sigma L/(\eta D_{\mathrm{th}})$. L is the characteristic length over the distance that σ varies by $\delta\sigma$, η, and D_{th} are the viscosity and the thermal diffusivity, respectively. This number is the ratio of the surface-tension driving force to the viscous dissipation force, so that if this number is larger than ~ 100, a stationary interface becomes unstable to surface tension-driven flow. Close to the critical point the surface tension vanishes with the universal form $\sigma = \sigma_0(T_c - T)^{2\nu}$, where $\nu = 0.63$ is a universal exponent, $\delta\sigma = -2\nu\sigma_0(T_c - T)^{2\nu-1}\,\delta T(\boldsymbol{x}) \sim (T_c - T)^{0.26}\,\delta T(\boldsymbol{x})$. The D_{th} factor in the denominator of Ma disappears with the form $D_{\mathrm{th}} \sim (T_c - T)^{0.85}$ [9] so that Ma has the form $\mathrm{Ma} \sim (T_c - T)^{-0.59}$, which diverges as $T \to T_c$. We note, however, that we do not have an externally imposed temperature gradient that corresponds to the classical Marangoni instability problem. A temperature gradient across the interface driven by evaporative heat transfer would tend to equilibrate any $\delta T(\boldsymbol{x})$ to maintain a uniform saturation pressure in the cell, i.e., local temperature perturbations away for an isothermal interface would be strongly dampened by evaporation. Even far from saturation, an evaporating interface tends to a uniform temperature through convective heat transport in the absence of an externally impose

temperature gradient, as observed in Ref. 7. In addition, the strength of any possible surface tension-driven convection is measured by the characteristic velocity $U \sim \delta\sigma/\eta$. This velocity goes to zero near T_c as $U \sim (T_c - T)^{0.26}$. Very close to the critical point, the velocity of the flow produced by a possible $\delta T(x)$ is probably too small to observe and certainly too small to drive the large bubble distortions that we have observed.

We next discuss the possible influence of the window tilt on the bubble shape. We first note that there are several important constraints present in our system. A liquid–gas mixture in coexistence has a specific volume fraction for gas given by the lever rule. The zero contact angle results in principal axes of curvature that are parallel to the cylinder axis, so that the edge of the bubble in Fig. 3 appears to be a thick dark line. These principal axes are oriented in a direction normal to this thick line. These regions of curved liquid–gas interface not in contact with the wall have a Laplace pressure $p = \sigma c$ at each element of free interface. Because both p and σ are constant on the interface, c is also constant at each point in this region.

We have computed the initial equilibrium bubble shape by minimizing the system's free energy as shown in Fig. 4a. This calculation used the Surface Evolver software, which employs the finite element method. We used a zero contact angle and a window tilt of 0.3°. This calculation matches the initial bubble shape, verifies that the bubble is touching the side wall, and verifies that the window tilts are the cause of this initial shape. To gain some qualitative understanding of this initial bubble shape we consider the forces on the bubble and the condition of mechanical equilibrium. The slight tilt of the windows about a tilt axis parallel to x by an angle θ makes a net reaction force from the windows in the $(-y)$ direction, as shown in Fig. 4b. The rotational symmetry that the bubble would have with parallel windows is broken in to a discrete reflection symmetry as the bubble changes from a circular cross section in the (x, y) plane to an oval cross section.

We first reduce this problem to two dimensions by integrating along all of the principal axes of the interface parallel to z to get net forces in the (x, y) plane as shown in Fig. 4. The y axis is in the reflection symmetry plane of the bubble (also the plane of maximum tilt that defines θ) and all of the x components of any normal or interfacial stress cancel by this reflection symmetry. At each element of the bubble between x and $x+dx$ there are several y components of force. There is the y component of the free interface, $F_{fI} \cos\phi$, which pushes in the $(-y)$ direction, where $F_{fI} = \sigma L$ and L is the distance between the windows, which depends on the shape of the bubble, $y(x)$. The flat tilted windows also produce a force, F_W, that pushes in the $(-y)$ direction, which is equal to $\int p \sin(\theta/2)\, l(x)\, dx$. The limits depend on the shape of the region in contact with the window that is parallel to the y axis, $l(x)$.

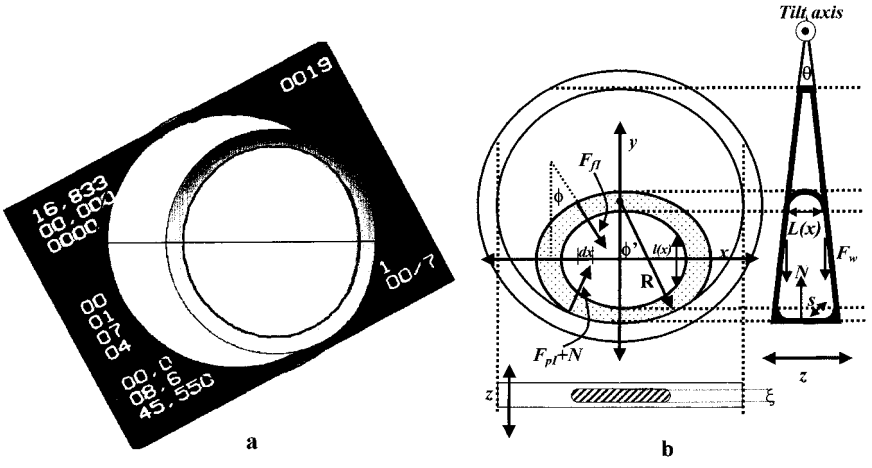

Fig. 4. The bubble in equilibrium. (a) Comparison of a 3-D numerical simulation of the equilibrium bubble shape with an actual image of the bubble. The numerical results (dark ovals) are drawn over the experimental images (also see Fig. 3). The image of the bubble interface is extrapolated to the actual edge of the cell, which is slightly outside of the field of view. The window tilt angle input to the simulation is 0.3°. (b) Diagram showing the forces on the bubble in equilibrium. The position of the bubble interface has coordinates x, y, and z, where y is the symmetry axis of the bubble and z is perpendicular to the image plane. In the (x, y) image plane is shown the free interface force, F_{fI}, which makes an angle, ϕ, with the y axis. Both the normal force from the side wall, N, and the pinned interface force, F_{pI}, make an angle ϕ' with the y axis. R is the radius of the cell and $l(x)$ is the width of the bubble along y. In the (y, z) slice at the right, the tilt angle, θ, the y component of the normal force from the window, F_w, the length of the pinned interface, s, and the width of the bubble along z, $L(x)$, are shown. At the bottom the other cross section in the (x, z) plane is shown, which shows the thickness, ξ, of the bubble–side wall contact area.

Below the x axis there are several forces that push the gas in the bubble in the $(+y)$ direction. The part that is not pinned by the wall has a $(+y)$ component to $F_{fI} \cos \phi$. The large curvature varies more strongly in this edge region of the bubble, and the small curvature also varies considerably in order to maintain the constant curvature condition. The part of the interface pinned by the wall has both normal and interfacial forces, which all push toward the center of the cell. The dark line corresponding to the interface is concentric with the cell radius so its large-curvature principal axis passes through the cylinder axis. This dark line is not as thick as it would be if it were not pinned by the side wall, implying that ξ, as defined in Fig. 4b, is constant as we have also seen in the numerical simulation. This pinned interface produces a force F_{pI} of constant magnitude that points toward the cell's center at each dx. This force is $\sigma s \cos \phi'$, where s is the length associated with the integration and ϕ' is the angle between the

cell radius and the y axis. There is also a normal force, $N = p\xi\, dx$, on the bubble from the side-wall region that is in contact with the bubble, as shown in Fig. 4.

Because the higher pressure in the bubble is caused by this Laplace pressure, $p = \sigma c$, all of the above forces are proportional to σ. All of these forces must also integrate to zero so that a constant σ on the isothermal interface factors out of the mechanical equilibrium condition and the bubble shape depends only on geometrical factors. The bubble shape should therefore also be independent of temperature. Although the window tilt and the constraining walls play an important roll in defining the boundary conditions and position of the bubble, they cannot be the cause of the bubble deformation that we have observed. As $\sigma(T)$ decreases when the bubble is heated, all the forces on the bubble decrease proportionately, i.e., the bubble become more easily deformed, but the reaction forces from the window tilt also decrease as the Laplace force decreases. We also note that in some experiments where the temperature was raised by steps and allowed to equilibrate between them, the bubble returned to its initial shape. We conclude that an external force is applied to this system as the heating is applied and the temperature is increased.

When very close to the critical point, the vapor bubble loses its convexity and evolves rapidly, as shown in Figs. 3D–H. As shown above, convective transport of heat cannot equilibrate the interface temperature. The other possible modes of heat transport are also very inefficient as $T \to T_c$. Temperature diffusion becomes low because $D_{th} \sim (T_c - T)^{0.85} \to 0$ as $T \to T_c$; the latent heat also goes to zero as $(T_c - T)^{\beta}$, where $\beta = 0.325$. In our experiment the cell is heated past T_c, so the possibility of $\delta T(x)$ along the interface increases close to T_c. There is, however, a very efficient heat transfer process close to the critical point. This process is an adiabatic heat transfer process caused by the diverging compressibility and thermal expansion coefficient particular to near-critical fluids [10]. The large thermal expansion and the slow diffusive transport of thermal energy in a near-critical fluid lead to a low-density thermal boundary layer near the heating walls. These expanded boundary layers compress the bulk fluid, heating it adiabatically. In a liquid–gas mixture, the compression by the boundary layer may heat the gas more than the liquid, leading to a quite large temperature difference [11]. Recently, in fact, it has been observed that when a two-phase system's temperature is quenched upward, the gas temperature may actually exceed the wall temperature [12]. Close to the critical point, a temperature change, $\delta T(x)$, where x is a position at the interface, could change the bubble's shape by producing a surface-tension change, $\delta\sigma$, on the interface. After the cell heating is started, the bubble deforms and the Laplace formula becomes $p = \sigma(x)\, c(x) = \text{constant}$. We

write $p = p_c + \delta p$ to separate the bulk pressure from the pressure caused by local variations of $\sigma(x)$ and $c(x)$. These quantities are also separated into local and bulk parts, i.e., $c(x) = c + \delta c(x)$ and $\sigma(x) = \sigma + \delta\sigma(x)$. Canceling the bulk part we find that $\delta c = ((\delta p/\delta\sigma) - c)/((\sigma/\delta\sigma) + 1)$. Because $\sigma/\delta\sigma \to 0$ as $T \to T_c$, the ratio $\delta p/\delta\sigma$ determines the near-critical behavior of δc. $\delta p/\delta\sigma$ measures the uniform pressure change when a surface-tension change occurs, and it is clear that $\delta p \to 0$ as $\delta\sigma \to 0$ (i.e., $T \to T_c$).

Near T_c the ratio $\delta p/\delta\sigma$ may either (i) diverge, (ii) converge to a constant, or (iii) converge to zero. In case (i) we find that $\delta c \sim \delta p(T_c - T)^{1-2\nu}$ as $T \to T_c$ so that the critical exponent for a curvature divergence would be weaker than $1 - 2\nu \approx -0.26$. Such a divergence of curvature probably occurred near the copper side wall. We have seen something quite opposite, in that the interface appears to flatten away from the side wall in some parts of Figs. 3F and G. This implies either that there is no curvature divergence [cases (ii) and (iii)] or that there is no $\delta T(x)$ along the interface in this region. On the other hand, if $\delta p/\delta\sigma \to c_0 = \text{constant}$ [case (ii)] or $\delta p/\delta\sigma \to 0$ [case (iii)] as $T \to T_c$, then $c(x) \to c_0$ or 0 as $T \to T_c$, i.e., a region of interface with a local change in temperature goes to this curvature value [case (ii)] or becomes flat [case (iii)] near the critical point. In cases (ii) and (iii), a $\delta T(x)$ along the interface could help to explain these images. At $T \geqslant T_c$, the surface tension vanishes, and the bubble's relaxation from surface tension is negligible, so that the "interface" shape is defined by local mass fluxes. In this case the interface evolution is analogous to the melting of a liquid–solid interface.

We next analyze another possible source of bubble deforming stress for an isothermal interface. The bubble may be deformed through the process of evaporation, i.e., by the normal stress exerted on the interface by the recoil from departing vapor [13, 14]. Let n be the evaporating mass per unit time per unit interface area. The evaporating gas moves normally to the interface, on average, and exerts a force per unit area (a "thrust") on the liquid of $\delta p(x) = n^2(x)((1/\rho_G) - (1/\rho_L))$, where ρ denotes the mass density and the subscripts L and G refer to liquid and gas, respectively. To find the distribution $n(x)$ at the interface it is necessary to solve the entire heat transfer problem, and this problem is complicated by the adiabatic heat transfer process. Because the temperature varies sharply in the boundary layer adjacent to the walls of the cell [10], the largest portion of mass transfer across the interface takes place near the triple contact line, so that $n(x)$ is large in the vicinity of the contact line. A more detailed analysis [15] shows that $n(x)$ can exhibit a logarithmic divergence at the contact line while decreasing exponentially far from it.

We assume that $n(x)$ has the following form: $n(x) = g(x)(T_c - T)^a$ as $T \to T_c$, i.e., it has the same local behavior with respect to temperature as

the critical temperature is approached. The rate of change of mass of the vapor bubble is $dM/dt = \int n(x)\, dx = d/dt(V\varphi\rho_G)$, where the integral is over the interfacial area, V is the cell volume, and φ is the constant-vapor volume fraction (φ is the ratio of the gas volume to the total volume, $\varphi = \frac{1}{2}$ when the average density is the critical density ρ_c). Near the critical point the coexistence curve has the form $\rho_G = \rho_c - \Delta\rho/2$, where $\Delta\rho \sim (T_c - T)^\beta$, with $\beta = 0.325$, so that $dM/dt \sim (T_c - T)^{\beta-1}\, dT/dt$ as $T \to T_c$. Thus, $a = \beta - 1$ and the curvature change due to the vapor recoil scales as $\delta c \sim \delta p/\sigma \sim (T_c - T)^{3\beta-2-2\nu}$. Because this critical exponent (≈ -2.3) is very large, it should manifest itself even far from the critical point in agreement with the experiments. This divergence is also much larger than the possible curvature divergence from a surface-tension gradient. In summary, as $T \to T_c$, the vapor mass growth follows the growth of its density (the vapor volume remains constant), so that the diverging vapor production near the critical point drives a diverging recoil force.

The shape of the interface is governed by the equation $\delta p(x) + p_c = c(x)\,\sigma$. Because c is proportional to the second derivative of the bubble shape, this governing formula is a differential equation with the boundary condition given by the actual contact angle. This actual contact angle is the first derivative of the bubble shape function at the solid wall and is zero near the critical point. This problem can be reduced to two dimensions as in the equilibrium case, and we solved it using an expression for $\delta p(x)$ that contains the main physical features of the solution of the heat conduction problem [15] (the logarithmic divergence at the contact line and the rapid decay away from it). The influence of the vapor recoil force relative to the surface tension is measured using a dimensionless parameter N, defined as $N = \int \delta p\, dl/\sigma$, where the integration is performed over the drop contour perpendicular to the contact line. Figure 5 shows how the apparent contact angle increases with the increase in N. Because $N \sim (T_c - T)^{-2.3} \to \infty$ as $T \to T_c$, the N increase mimics the approach to the critical point and qualitatively explains the observed shape of the vapor bubble. The large apparent contact angle can be understood by noting that the curvature increases sharply near the contact line. Because the interface slope changes so abruptly near the contact line, the contact angle appears much larger than zero, as shown in Fig. 5. In other experiments [16] under weightless conditions a similar drying process can be seen in the bubble images. Multiple bubble interactions and a low cell aspect ratio, however, complicated these experiments.

A very similar drying takes place during the liquid boiling process at a large heat flux. When the heating to a surface is increased past a critical heat flux, there is a sudden transition to "film" boiling, where the heater becomes covered with gas and may burn out [14, 15]. This "burnout" or

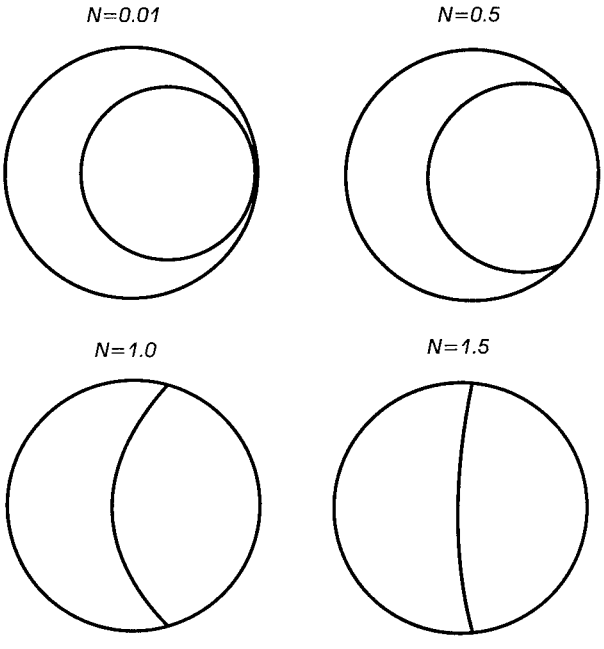

Fig. 5. Calculated contact angle and bubble shape. The calculated shape of the vapor–liquid interface as described in the text for the different values of the dimensionless strength of vapor recoil N, which goes to infinity when the system approaches the critical point. Note that the actual contact angle is zero for all the curves.

"boiling crisis" is an important practical problem in many industries. We interpret the boiling crisis to be similar to the drying transition shown here [15]. Recent numerical calculations also support this interpretation [17]. The main difference is that the large value of N is made by a large vapor production that can be achieved during strong overheating rather than by the critical effects.

ACKNOWLEDGMENTS

This work was supported by CNES and NASA OBPS Grant NAG3-1906. We thank all of the Alice-II team, especially J. F. Zwilling, and all individuals involved in the Mir missions for their technical support.

REFERENCES

1. L. S. Tong, *Boiling Heat Transfer and Two-Phase Flow* (Taylor & Francis, New York, 1997).
2. M. R. Moldover, J. V. Sengers, R. W. Gammon, and R. J. Hocken, *Rev. Mod. Phys.* **51**:79 (1979).
3. P.G. De Gennes, *Rev. Mod. Phys.* **57**:827 (1985).
4. C. Morteau, M. Salzman, Y. Garrabos, and D. Beysens, in *Proceedings of the 2nd European Symposium on Fluids in Space,* A. Viviani, ed. (Congressi srl, Rome, 1997), p. 327.
5. J. P. Delville, C. Salzman, Y. Garrabos, and D. Beysens, in *Proceedings of the 2nd European Symposium on Fluids in Space,* A. Viviani, ed. (Congressi srl, Rome, 1997), p. 312. Also see J. Hegseth, *Bull. Am. Phys. Soc.* **43**:2036 (1998).
6. J. R. A. Pearson, *J. Fluid Mech.* 4:489 (1958).
7. J. Hegseth, N. Rashidnia, and A. Chai, *Phys. Rev. E* **54**:1640 (1996).
8. S. H. Davis, *Annu. Rev. Fluid Mech.* **19**:403 (1987).
9. P. Jany and J. Straub, *Int. J. Thermophys.* **8**:165 (1987).
10. Y. Garrabos, M. Bonetti, D. Beysens, F. Perrot, T. Frohlich, P. Carles, and B. Zappoli, *Phys. Rev. E* **57**:5665 (1998), and references therein.
11. J. Straub, L. Eicher, and A. Haupt, *Phys. Rev. E* **51**:5556 (1995).
12. R. Wunenburger, Y. Garrabos, C. Lecoutre-Chabot, D. Beysens, and J. Hegseth, *Phys. Rev. Lett.* **84**:4100 (2000).
13. H. J. Palmer, *J. Fluid. Mech.* **75**(3):487 (1976).
14. J. Straub, in *Proceedings of the IXth European Symposium on Gravity-Dependent Phenomena in Physical Sciences,* L. Rathe, H. Walter, and B. Feuerbacher, eds. (Springer, Berlin, 1995), p. 351.
15. V. S. Nikolayev and D. Beysens, *Europhys. Lett.* **47**:345 (1999).
16. C. Ikier, H. Klein, and D. Woermann, *J. Colloid Interface Sci.* **178**:368 (1996).
17. V. S. Nikolayev, D. A. Beysens, G. L. Lagier, and J. Hegseth, *Int. J. Heat Mass Transfer* **44**:99 (2001).